Research Article

Journal of
Environmental
Nanotechnology

In-Situ ZnO Nanoparticles on Lyocell Fabric for Antibacterial and UV Protection

K. V. Arunkumar[1*], K. M. Pachiyappan[1], M. Balaji[2], C. K. M. Thayalan[2] and S. Gayathri[2]
[1]Department of Costume Design and Fashion, PSG College of Arts and Science, Coimbatore, TN, India
[2]Department of Biotechnology, PSG College of Arts and Science, Coimbatore, TN, India
Received: 05.07.2026 Accepted: 09.08.2026 Published: 30.09.2026
*kvaruncdf@gmail.com

ABSTRACT

Lyocell is a sustainable regenerated cellulose fiber that has excellent comfort characteristics but lacks antibacterial and UV protection properties. The present study was performed to develop multifunctional lyocell fabrics through in situ synthesis of zinc oxide (ZnO) nanoparticles to improve antibacterial and UV-protective performance. Citric acid was used to pre-treat the lyocell fabric, and the in-situ synthesis of ZnO nanoparticles was performed by using the zinc acetate precursor concentrations of 0.25 M (L1) and 0.5 M (L2). The properties of treated fabrics were analysed using FTIR, FESEM-EDS, and XRD, while the functional performance was assessed by antibacterial activity, ultraviolet protection factor (UPF), and air permeability. The characterization analysis results confirmed successful synthesis of ZnO nanoparticles, which were uniformly deposited on the lyocell surface without destroying the cellulose structure. By increasing the concentration of the precursor, zinc content rose from 7.32 wt % (L1) to 20.34 wt % (L2), which enhanced the deposition of ZnO. Similarly, the L2 fabric exhibited a better antibacterial effect, with inhibition zones of 6.29 mm for *Staphylococcus aureus* and 6.69 mm for *Escherichia coli*, whereas the L1 fabric showed about 4.13 mm and 4.22 mm, respectively. The UPF of the pristine lyocell was significantly improved to 18.2 (L1) and 26.9 (L2), while the air permeability was moderately reduced from 232 mm/s down to 176 mm/s, indicating a better performance without significantly sacrificing breathability. The results indicate that the in situ ZnO functionalization method is an efficient and eco-friendly process for obtaining multifunctional lyocell fabrics with improved antibacterial and UV protection. The developed materials have shown great potential for application in medical, protective, sportswear, and other advanced technical textile products. Washing durability, long-term stability, and large-scale industrial implementation should be the focus of future studies.

Keywords: ZnO nanoparticles; In-Situ synthesis; Lyocell fabric; Nanofinishing.

1. INTRODUCTION

The accelerating demand for sustainable yet high-performance textile materials has sharpened research interest in regenerated and bio-based fiber platforms, as well as in advanced surface functionalization strategies capable of delivering durable added value beyond comfort and aesthetics (Abou *et al.* 2022). Among regenerated cellulosic fibers, lyocell has gained prominence because it is produced via a direct dissolution route and is often cited as a comparatively resource-conserving, lower-impact alternative to other regenerated-cellulose technologies. The lyocell process has been widely characterized as benefiting from solvent recovery, recycling, and industrial viability (Ivanova *et al.* 2026). In addition to this process advantage, lyocell-based textiles are valued for their mechanical robustness, moisture-related comfort performance, and biodegradation potential, supporting their adoption in apparel and increasingly in hygiene and technical textile segments (Rodrigues *et al.* 2025).

Despite these merits, like other cellulosic fibers, lyocell does not inherently possess antimicrobial or protective properties, which limits its use in hygiene and high-performance applications where microbial contamination, odor formation, or infection control are key factors (Mondal, 2022; Wendler *et al.* 2024). Recent advances in nanotechnology have enabled the development of multifunctional textile surfaces with antimicrobial, UV-protective, and self-cleaning properties (Abou *et al*. 2022; Mondal, 2022). In parallel, environmentally benign approaches employing plant-derived materials have gained attention as sustainable routes for the synthesis of metal-oxide nanoparticles, as demonstrated for TiO_2 nanoparticles synthesized using *Leucas aspera* leaf extract (Blessymol *et al*. 2023).

Zinc oxide (ZnO) nanoparticles have become one of the most extensively studied metal oxides for multifunctional textile finishing, owing to their combined antibacterial efficacy, UV-blocking capability, and photocatalysis-related self-cleaning potential (Verbič *et al.* 2019). Additionally, ZnO also benefits from a favorable safety and regulatory profile; notably, zinc oxide is listed as "generally recognized as safe" (GRAS) when used in accordance with good manufacturing practice, strengthening the rationale for ZnO-based

finishes in protective and near-skin textile applications (Ravi and Babu, 2025).

Conventional ex-situ strategies such as external binder-based coatings or post-synthesis deposition often suffer from nanoparticle aggregation and insufficient interfacial adhesion, resulting in gradual loss of functionality under repeated laundering and wearing in the consumer phase (Jalali *et al.* 2024; Shilo and Tarangini, 2023). In contrast, in-situ synthesis, wherein ZnO is nucleated and grown directly on the fiber surface, is increasingly favoured because it promotes more homogeneous coverage and stronger interfacial coupling, thereby improving durability (Mpofu *et al.* 2025).

For cellulosic substrates, surface activation is critical for improving nanoparticle fixation by increasing the availability of chemical anchoring sites (Djafari *et al.* 2023). In regenerated cellulose systems such as lyocell, this approach is particularly effective due to the fiber's well-defined morphology, high crystallinity, and abundance of hydroxyl groups, which can act as active binding sites for metal ions (Wang *et al.* 2024). However, to further enhance nanoparticle immobilization and durability, especially under wet-use and laundering conditions, additional surface modification strategies are often required (Periyasamy, 2022; Sadannavar *et al.* 2024). In this context, poly (carboxylic acid) crosslinking, particularly via citric acid, has emerged as a sustainable and environmentally benign approach. Citric acid introduces additional carboxyl functional groups onto the cellulose backbone, thereby increasing the density of coordination sites for metal ions and significantly improving nanoparticle fixation and stability (Xu *et al.* 2024).

Pre-treatment approaches, including the use of organic acids or mordant-like systems, further enhance metal-ion adsorption and promote uniform nanoparticle nucleation on the fiber surface (Periyasamy, 2022; Sadannavar *et al.* 2024). These treatments not only enhance interfacial interactions between the substrate and metal precursors but also facilitate the controlled growth of nanoparticles, leading to improved functional performance. Such strategies are especially relevant for lyocell, whose physicochemical characteristics differ from those of conventional cotton, necessitating tailored surface-engineering approaches.

Previous studies demonstrated successful in-situ ZnO deposition primarily on cotton substrates with improved antibacterial and UV-protective properties. (Javed *et al.* 2021; Verbič *et al.* 2021). However, they did not systematically investigate regenerated lyocell substrates or evaluate concentration-dependent nanoparticle growth and its correlation with multifunctional performance. The present study addresses these limitations through citric acid-assisted in situ ZnO synthesis on lyocell fabric and comprehensive structural and functional characterization.

The study's research gap was that ZnO nanoparticle functionalization has been extensively investigated on cotton and other natural textiles; comparatively few studies have focused on regenerated cellulose fibres, such as lyocell, using an in-situ synthesis approach. Existing studies primarily report antibacterial or UV-protective performance but rarely investigate how ZnO precursor concentration affects nanoparticle growth, structural characteristics, and multifunctional textile performance. Furthermore, sustainable, binder-free surface activation strategies to improve nanoparticle anchoring remain underexplored.

The novelty of this work lies in the binder-free in situ synthesis of ZnO nanoparticles on lyocell fabric via citric acid-assisted surface activation. The study systematically correlates ZnO precursor concentration with nanoparticle deposition, FTIR, FESEM-EDS, XRD, antibacterial activity, UV protection, and air permeability, thereby establishing a clear structure-property relationship for sustainable multifunctional lyocell textiles.

2. MATERIALS AND METHODS

2.1 Materials

The in situ formation of zinc oxide nanoparticles was performed on a woven lyocell fabric manufactured from 40s-count yarns, with a construction of 132 ends per inch and 72 picks per inch, corresponding to a fabric mass of 130 $g \cdot m^{-2}$. The fabric exhibited a 2/1 twill weave structure, which provides an appropriate balance between surface area and mechanical stability for nanoparticle deposition. Zinc acetate dihydrate (analytical grade) was employed as the precursor for Zn^{2+} ions, while NaOH served as the precipitating agent for the formation of ZnO nanoparticles. All chemicals used in the study were of laboratory reagent grade and were utilized without further purification. Distilled water was used throughout the experimental procedure to ensure consistency and to avoid interference from ionic impurities.

Zinc acetate precursor concentrations of 0.25 M and 0.5 M were selected to evaluate the effect of precursor concentration on the in-situ formation of ZnO nanoparticles on lyocell fabric. A concentration of 0.25 M was expected to promote controlled nucleation and uniform nanoparticle deposition, whereas 0.5 M was chosen to increase ZnO loading, thereby enhancing multifunctional properties. Higher precursor concentrations were not considered because they may lead to excessive particle agglomeration, non-uniform coatings, blockage of fabric pores, and deterioration of

fabric comfort. Therefore, these two concentrations were considered sufficient to investigate the concentration-dependent performance of ZnO-functionalized lyocell within the scope of this work. Three experimental groups were prepared for the study, namely pristine lyocell fabric (L), lyocell treated with 0.25 M ZnO precursor (L1), and lyocell treated with 0.5 M ZnO precursor (L2). Each treatment was independently prepared to ensure reproducibility of the experimental results. All quantitative experiments were expressed as mean ± standard deviation. One-way ANOVA with Tukey's post hoc test assessed differences among untreated and ZnO-treated samples with $p < 0.05$ considered statistically significant.

2.2 Pre-treatment of Lyocell Fabric

Prior to nanoparticle synthesis, the lyocell fabric underwent pretreatment to remove any added or natural impurities, residual waxes, and spin-finishing agents that could hinder nanoparticle formation and uniform distribution. Scouring was performed using a non-ionic detergent solution (2 g/L) at 60 °C for 30 min, maintaining a material-to-liquor ratio of 1:30. Following treatment, the fabric was thoroughly rinsed with distilled water to remove residual chemicals and subsequently air-dried. To enhance the affinity of the lyocell substrate toward metal ions, the scoured fabric was pre-treated with a 5 wt% citric acid solution (Figure 1.1). The treatment was carried out at 60 °C for 30 min, after which the samples were dried in a hot air oven at 80 °C. This pre-treatment step facilitates the introduction of additional carboxyl functional groups onto the lyocell surface, thereby improving zinc ion adsorption through coordination interactions. Also, citric acid plays a dual role as a crosslinking and anchoring agent between lyocell cellulose and ZnO nanoparticles. Consequently, this modification significantly enhances nanoparticle nucleation, fixation, and overall stability on the lyocell matrix during subsequent in situ synthesis.

2.3 ZnO Nanoparticles on Lyocell Fabric

The in situ synthesis of ZnO nanoparticles on lyocell fabric was carried out by chemical precipitation. Zinc acetate solutions (0.25 M and 0.5 M) were prepared in distilled water and continuously stirred to ensure complete dissolution (Figure 1, 2 & 3). The pre-treated lyocell fabric samples were immersed in the solution for 45 min to facilitate the adsorption of Zn^{2+} ions onto the fiber surface through interactions with hydroxyl and carboxyl functional groups. Subsequently, a 1 M sodium hydroxide solution was added dropwise to the reaction bath until an alkaline pH of approximately 9–10 was reached, promoting the formation of zinc hydroxide as a white, gelatinous precipitate anchored to the fiber surface. The reaction was maintained at 70–80 °C for 60 min to support the nucleation and growth of nanoparticles directly on the lyocell fabric (Figure 1.4). During this process and subsequent autoclaving, the initially formed zinc hydroxide underwent thermal dehydration, yielding crystalline ZnO nanoparticles. Following synthesis, the treated fabric was thoroughly rinsed with distilled water to remove residual chemicals and air-dried. Overall, the process involves the transformation of zinc acetate and sodium hydroxide into ZnO nanoparticles on the lyocell surface, with concurrent formation of sodium acetate and water, while the fiber matrix facilitates nanoparticle nucleation, anchoring, and stabilization (Figure 1.5). Figure 2 presents a schematic workflow illustrating ZnO nanoparticle deposition on lyocell fabric.

$$\text{Cell–OH} + \text{HOOC–R–COOH} \rightarrow \textbf{Cell–O–CO–R–COOH} + \textbf{H}_2\textbf{O} \quad (1)$$

$$Zn(CH_3COO)_2{\cdot}2H_2O \rightarrow Zn^{2+} + 2CH_3COO^- + 2H_2O \quad (2)$$

$$Zn^{2+} + 2OH^- \rightarrow Zn(OH)_2 \downarrow \quad (3)$$

$$Zn(OH)_2 \rightarrow ZnO + H_2O \quad (4)$$

$$\text{Cell–OH / Cell–COO}^- + Zn^{2+} \rightarrow \textbf{Cell–O–Zn}^{2+} \quad (5)$$

Fig. 1: Chemical reaction for in-situ synthesis of ZnO nanoparticles on lyocell fabric

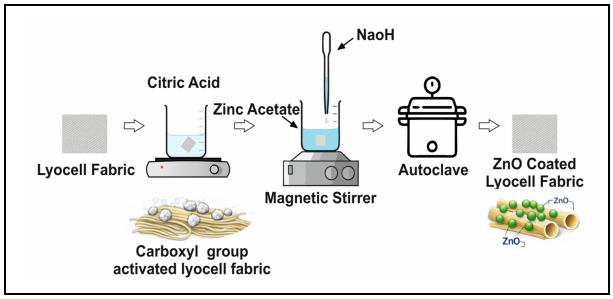

Fig. 2: Schematic workflow of ZnO nanoparticle deposition on lyocell

2.4 Characterization of ZnO Nanoparticle Deposition on Lyocell Fabric

Fourier transform infrared spectroscopy (FTIR) analysis was used to confirm ZnO nanoparticle formation and functional groups (4000–400 cm^{-1}). Field emission scanning electron microscopy (FESEM) with a palladium coating was used to examine surface morphology and nanoparticle distribution, while EDS verified the Zn and O composition and uniformity. The crystalline structure of pristine lyocell and ZnO-coated lyocell fabrics was analyzed using an X-ray diffractometer equipped with Cu Kα radiation (λ = 1.5406 Å), operating at 45 kV and 30 mA. Diffraction patterns were recorded over a 2θ range of 10°–80° using appropriate scanning steps and scan rates. The obtained diffraction peaks were indexed by comparison with the standard JCPDS card (No. 36-1451) for hexagonal wurtzite ZnO.

The average crystallite size of the synthesized ZnO nanoparticles was estimated using the Debye–Scherrer equation (Equation 6):

$$D = \frac{K\lambda}{\beta cos\theta} \quad \ldots (6)$$

Where,

- **D** = crystallite size (nm)
- **K** = shape factor (0.9)
- **λ** = X-ray wavelength (1.5406 Å, Cu Kα)
- **β** = FWHM (radians)
- **θ** = Bragg angle

The crystallite size was calculated using the prominent ZnO diffraction peaks, and the average value was reported.

UPF (AATCC 183:2010) was measured after conditioning using UV–Vis spectrophotometry (280–450 nm), with multiple measurements ensuring accuracy and accounting for fabric heterogeneity. The UPF of each fabrics calculated using the standard equation (Equation 7), which integrates the erythemal weighted irradiance and spectral transmittance across the UV range.

$$UPF = \frac{\sum_{\lambda=280}^{\lambda=400} E\lambda \cdot S\lambda \cdot \Delta\lambda}{\sum_{\lambda=280}^{\lambda=400} E\lambda \cdot S\lambda \cdot T\lambda \cdot \Delta\lambda} \quad \ldots (7)$$

where E_λ: is the solar UVR spectral irradiance in $W.m^{-2}\ nm^{-1}$

S_λ: solar spectral irradiance in $W.m^{-2}\ nm^{-1}$

T_λ: spectral transmittance of fabric (%)

Δ_λ: the wavelength interval of the measurement in nm (5 nm),

λ: the wavelength in nm (290-400 nm).

2.4.1 Antimicrobial Activity Assessment

Antibacterial activity of the lyocell samples was evaluated using both agar diffusion and AATCC 100 quantitative methods. For the agar diffusion assay, Mueller-Hinton agar plates were prepared and uniformly inoculated with 100 µL of bacterial suspension adjusted to 0.5 McFarland standard (0.15 OD). The study was conducted against *Staphylococcus aureus* and *Escherichia coli*. Fabrics of (2×1 cm), including pristine lyocell (L) and ZnO nanoparticle-treated samples, were aseptically placed on the inoculated agar surface and incubated at 37 °C for 24 h. The antibacterial efficacy was assessed by measuring the diameter of the inhibition zones. In addition, quantitative antibacterial activity was determined using the AATCC 100 standard method, in which the reduction in bacterial count (CFU/mL) after contact with the fabric was calculated. All experiments were performed in triplicate, and mean values were reported.

2.4.2 Air-permeability Measurement

The air permeability of pristine lyocell and ZnO nanoparticle-treated fabrics was measured in accordance with ISO 9237:1995 at a pressure of 100 Pa. Samples were conditioned (20±2°C, 65±2% RH, 24 h). Airflow rate (mm/s) was recorded. Five measurements per sample (L, L1, L2) were averaged to ensure accuracy and reproducibility under controlled testing conditions. All measurements were conducted in triplicate (n=3) and expressed as mean ± standard deviation. One-way ANOVA with Tukey's post hoc test assessed differences among samples, with $p < 0.05$ considered statistically significant.

3. RESULTS AND DISCUSSION

3.1 FTIR Analysis

Fourier transform infrared (FTIR) spectroscopy was employed to confirm the in-situ formation of ZnO nanoparticles on lyocell fabric and to evaluate possible chemical interactions between the deposited inorganic phase and the cellulose matrix (Figure 3). The spectra of pristine lyocell (L), ZnO-treated lyocell prepared with 0.25 M zinc acetate precursor (L1), and ZnO-treated lyocell prepared with 0.5 M precursor concentration (L2) were compared to assess structural changes after treatment. The pristine lyocell fabric (L) exhibited the characteristic absorption profile of regenerated cellulose, confirming the integrity of the cellulose backbone (Cichosz and Masek, 2020; Geminiani *et al.* 2022). A broad absorption band in the high-wavenumber region, centered around 3641 cm^{-1}, was assigned to O–H stretching vibrations associated with hydroxyl groups involved in extensive intra- and intermolecular hydrogen bonding within the cellulose structure. The band observed at 2978 cm^{-1} corresponded to C–H stretching vibrations of aliphatic groups in the anhydroglucose units. In the fingerprint region, the intense band near 1056 cm^{-1} was attributed to C–O stretching and C–O–C vibrations of the cellulose framework, which are typical of regenerated cellulose and indicative of the preserved cellulose I-related structure of lyocell fibers (Liu and Kim, 2017).

After the in-situ ZnO treatment, the major cellulose absorption bands are visible in both L1 and L2 spectra, indicating that the nanoparticle synthesis process did not significantly alter the fundamental chemical structure of the lyocell substrate. This observation is important because it demonstrates that the treatment was predominantly a surface modification rather than a destructive chemical transformation of the cellulose matrix. Nevertheless, distinct spectral changes were observed in the treated samples, confirming the successful incorporation of ZnO nanoparticles. The most significant evidence for ZnO formation appeared in the low-wavenumber region, where an absorption band at approximately 447-460 cm^{-1} was observed in both L1 and L2. This band is attributed to Zn–O stretching vibrations and is widely recognized as a characteristic signature of zinc oxide. The appearance of this peak in the treated fabrics, together with its absence in the untreated sample, confirms the successful formation and deposition of ZnO nanoparticles on the lyocell surface (Sowri *et al.* 2013).

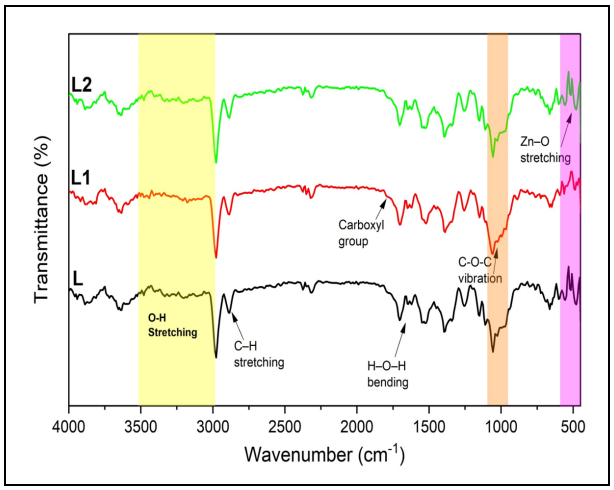

Fig. 3: FTIR spectra of pristine lyocell (L) and ZnO treated lyocell sample (L1, L2)

A comparative analysis of the treated samples further revealed that the intensity of the Zn–O absorption band increased from L1 to L2, indicating a concentration-dependent enhancement in nanoparticle deposition. This suggests that increasing the precursor concentration from 0.25 M to 0.5 M promoted greater ZnO formation and higher surface loading on the fabric. In addition to the Zn–O band, subtle modifications were observed in the O–H stretching region of the treated samples, including slight broadening and variations in band intensity. These changes may be attributed to interactions between Zn^{2+} species or ZnO nanoparticles and the hydroxyl groups of cellulose, which can modify the hydrogen-bonding environment of the fiber surface. Such interactions are consistent with the role of cellulose hydroxyl groups in facilitating adsorption, nucleation, and anchoring of ZnO nanoparticles during in situ synthesis.

The citric acid pre-treatment introduces carboxyl groups onto the lyocell surface; this confirms there is a small peak in the carbonyl region around 1700–1750 cm^{-1}, suggesting coordination between Zn^{2+} ions and carboxyl functionalities. Although these changes may be less pronounced than the Zn–O vibration, they support the hypothesis that surface functional groups contribute to the immobilization and stabilization of nanoparticles on the cellulose matrix. Minor variations in the cellulose fingerprint region, particularly within the 1000–1200 cm^{-1} range, may also arise from nanoparticle coverage and interfacial interactions, although the persistence of the principal cellulose bands confirms that the polysaccharide backbone remains intact (Sowri *et al.* 2013).

Overall, the FTIR results demonstrate that ZnO nanoparticles were successfully synthesized in situ on the lyocell fabric without compromising the molecular structure of the cellulose substrate. The retention of characteristic cellulose bands confirms structural preservation, while the emergence of the Zn–O stretching band provides direct evidence of nanoparticle formation. The stronger Zn–O signal in L2 relative to L1 further verifies that ZnO deposition increased with precursor concentration. These findings confirm the effectiveness of the in-situ synthesis approach for producing ZnO-functionalized lyocell fabrics with preserved fiber chemistry and enhanced surface functionality.

3.2 Surface Morphology and EDS Elemental Analysis

Zinc oxide nanoparticle production and distribution on the fiber surface were assessed by analyzing the surface morphology of pristine lyocell fabric (L) and samples treated with ZnO nanoparticles (L1 and L2) using FESEM. The FESEM image of the pristine lyocell fabric (L) shows a smooth, uniform, and well-defined fiber surface with a typical longitudinal structure of regenerated cellulose fibers (Figure 4a). The absence of surface deposits or particulate matter confirms that the pristine lyocell fabric possesses a clean and compact morphology. Such smooth surface characteristics are commonly observed in regenerated cellulose fibers due to their high crystallinity and uniform structure. On the other hand, compared to the control, the ZnO-treated sample L1 (0.25 M) clearly shows surface alteration (Figure 4b). Fine granular and clustered nanoparticle deposits are visible throughout the fiber surface, as seen in the FESEM micrograph. A successful nucleation and development of ZnO nanoparticles using the in-situ synthesis approach is indicated by the homogeneous anchoring of these nanoparticles along the longitudinal direction of the fibers. According to the comparatively even distribution, Zn^{2+} ions and the hydroxyl groups of lyocell fibers interact effectively to promote the production and attachment of nanoparticles.

ZnO nanoparticle deposition on the lyocell surface is more noticeable in the L2 sample (0.5 M). In comparison to L1, the FESEM image shows a higher density of nanoparticles with larger agglomerated clusters (Figure 4c). Higher nanoparticle loading gives the fiber surface a rougher, more textured appearance. This increased deposition demonstrates that ZnO nanoparticle nucleation and development on the fiber surface are enhanced by higher precursor concentrations. Similar findings have been seen in cases where a larger concentration of the precursor led to improved functional performance and a greater coverage of nanoparticles.

Overall, FESEM analysis confirms the successful in situ formation and deposition of ZnO nanoparticles on lyocell fabric. The transition from a relatively smooth surface in the pristine lyocell sample to a rough, nanoparticle-coated morphology in treated samples evidences effective nucleation and anchoring. Moreover, the higher nanoparticle density observed in L2 compared to L1 indicates concentration-dependent growth, which is expected to enhance the antimicrobial and protective performance of the fabric. These findings validate the efficiency of the in-situ synthesis approach for developing durable, eco-functional lyocell textiles.

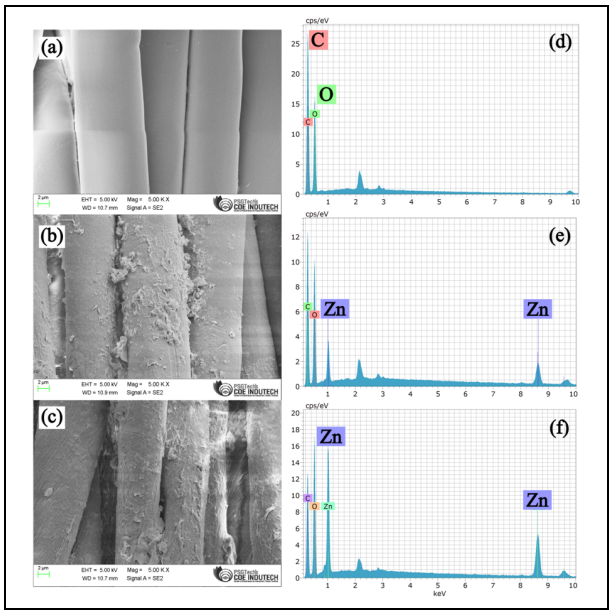

Fig. 4: FESEM image of control sample L (a); ZnO nanoparticle deposits on lyocell L1 (b); L2 (c); EDS spectrum control sample L (d); presence of Zn and O on L1 (e) and L2 (f)

EDS was employed to determine the elemental composition of pristine lyocell fabric (L) and ZnO-treated samples prepared with 0.25 M (L1) and 0.5 M (L2) precursor concentrations, thereby confirming the formation and deposition of ZnO nanoparticles. The EDS spectrum of the control sample (L) revealed only carbon (C) and oxygen (O), with weight percentages of 53.05% and 46.95%, respectively, corresponding to the intrinsic composition of cellulose (Figure 4d). The absence of zinc peaks in this sample confirms the purity of the pristine lyocell substrate and provides a reliable baseline for comparison. In contrast, the ZnO-treated samples (L1 and L2) exhibited the presence of zinc in addition to carbon and oxygen, clearly indicating successful nanoparticle formation on the fiber surface. For sample L1 (0.25 M), the elemental composition included 7.32 wt% Zn, along with contributions from carbon (23.47 wt%) and oxygen (17.93 wt%), demonstrating effective nucleation and moderate deposition of ZnO nanoparticles (Figure 4e). In sample L2 (0.5 M), a significant increase in zinc content (20.34 wt%) was observed, accompanied by 25.90 wt% oxygen, confirming enhanced nanoparticle growth and higher surface loading at increased precursor concentration (Figure 4f).

Comparative analysis reveals a clear concentration-dependent trend in ZnO deposition, with zinc content progressively increasing from L1 to L2. The simultaneous detection of zinc and oxygen in treated samples further confirms the formation of ZnO rather than metallic zinc. Additionally, the persistence of carbon signals across all samples indicates that the cellulose matrix remains intact during the in-situ synthesis process. Overall, the EDS results validate the effectiveness of the synthesis method, demonstrating successful and tunable deposition of ZnO nanoparticles on lyocell fabric, which is essential for enhancing its functional properties.

3.3 XRD Analysis

The X-ray diffraction (XRD) patterns shown in the figure clearly distinguish the crystalline characteristics of pristine lyocell (L) and ZnO-treated lyocell (L2), providing strong evidence of structural modification induced by the in-situ nanoparticle synthesis. A detailed comparison reveals the coexistence of preserved cellulose crystalline domains and newly introduced ZnO nanocrystalline phases, demonstrating the formation of a robust organic–inorganic hybrid system (Figure 5). The diffraction profile of pristine lyocell (L) exhibits a broad semi-crystalline pattern dominated by a pronounced peak around 2θ between 20–22°, which is typically associated with the (200) plane of regenerated cellulose in the form of the cellulose II structure. This peak represents the ordered arrangement of cellulose chains stabilized through intra and intermolecular hydrogen bonding. The broad nature of the peak also indicates the presence of significant amorphous regions, which is characteristic of lyocell fibers. A low-intensity shoulder at lower angles at the 2θ between 12–14° further confirms partial crystallinity, reflecting disordered domains within the lyocell fiber matrix.

On the other hand, the ZnO-treated sample (L2) exhibits a distinctly different diffraction profile that reflects the emergence of a second crystalline phase

(Figure 5). While the cellulose peak around 20–22° is still present in L2, its relative intensity appears reduced and slightly broadened compared to the pristine sample. This observation suggests that the in-situ ZnO growth induces subtle disruption in the hydrogen-bonded network of cellulose, likely at the surface level. Such changes indicate a partial reduction in crystallinity or increased structural heterogeneity due to nanoparticle incorporation and interfacial interactions.

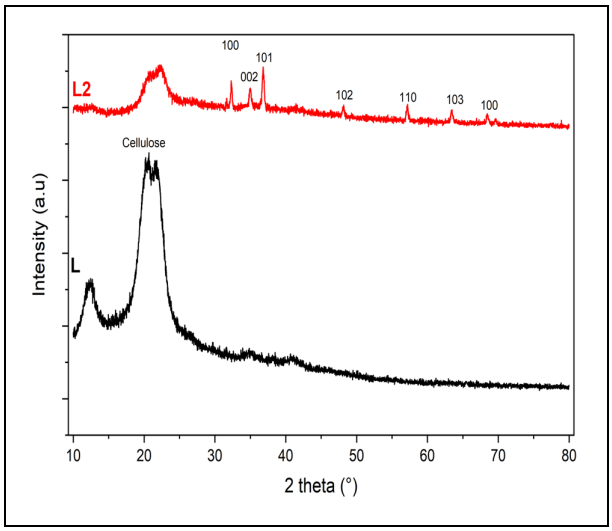

Fig. 5: XRD analysis of pristine lyocell (L) and ZnO-treated lyocell sample (L2)

Table 1. Crystallite size of ZnO nanoparticles calculated using the Debye–Scherrer equation

Peak No.	2θ (°)	Plane (hkl)	FWHM (°)	d-spacing (Å)	Crystallite Size (nm)
1	31.63	100	0.2007	2.8289	42.95
2	36.91	101	0.1004	2.4354	87.09
3	48.21	102	0.1338	1.8875	67.91
4	57.17	110	0.2007	1.6113	47.06
5	63.36	103	0.2676	1.4679	36.42
6	68.47	112	0.2342	1.3703	42.84
7	69.62	201	0.2676	1.3505	37.75
Average ± SD					51.72 ± 18.80

More importantly, the L2 pattern displays several sharp diffraction peaks in the higher 2θ region (30°–70°), which are completely absent in the pristine lyocell spectrum. The crystallite size of the ZnO nanoparticles was estimated using the Debye–Scherrer equation from the major diffraction peaks of hexagonal wurtzite ZnO. As presented in Table 1, the crystallite size ranged from 36.42 to 87.09 nm, with an average crystallite size of 51.72 ± 18.80 nm. The observed variation in crystallite size among different crystallographic planes is attributed to differences in peak broadening and crystal growth along specific orientations. The nanoscale crystallite size confirms the successful in-situ formation of crystalline ZnO nanoparticles on the lyocell fabric surface.

The structural evolution observed in L2 arises from the strong interaction between Zn^{2+} precursor ions and the hydroxyl (-OH) functional groups of lyocell. These hydroxyl groups serve as active nucleation sites for ZnO, enabling localized growth directly on the fiber surface. This leads to the formation of anchored ZnO nanocrystals that are structurally integrated rather than physically deposited. The slight reduction in cellulose peak intensity and increased baseline scattering supports this interfacial modification, indicating partial disruption or reorganization of surface crystalline domains.

3.4 Antimicrobial Analysis

The antibacterial performance of pristine lyocell (L) and ZnO-functionalized fabrics (L1, L2) was evaluated against *Staphylococcus aureus* and *Escherichia coli* using the agar diffusion method, it can be seen in Figure 6. Pristine lyocell showed no inhibition (0 mm), confirming the absence of intrinsic antimicrobial activity due to its hydrophilic cellulose structure. In contrast, ZnO-treated samples exhibited clear antibacterial effects. L1 (0.25 M) showed inhibition zones of 4.13 mm (S. *aureus*) (Figure 6a) and 4.22 mm (*E. coli*), while L2 (0.5 M) demonstrated enhanced activity with 6.29 mm and 6.69 mm, respectively (Figure 6b). This indicates a concentration-dependent antibacterial effect. The slightly higher inhibition against *E. coli* is attributed to its thinner cell wall, allowing easier penetration of ZnO nanoparticles and reactive species. Overall, increased ZnO loading significantly improves the bactericidal performance of lyocell fabrics.

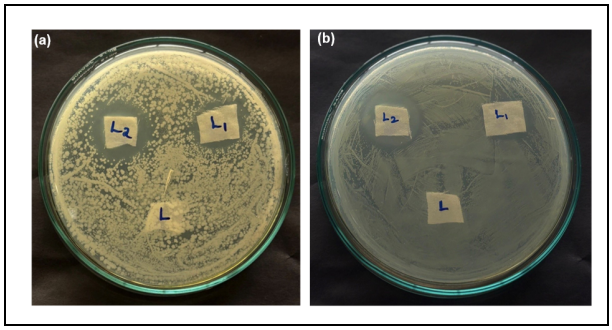

Fig. 6: Antimicrobial activity of pristine lyocell (L) and ZnO-treated lyocell sample (L1, L2); *Staphylococcus aureus* (a) and *Escherichia coli* (b)

Antibacterial inhibition zone measurements were performed in three independent replicates (n = 3). The results are expressed as mean ± standard deviation. Statistical significance between untreated and ZnO-treated samples was determined using one-way ANOVA followed by Tukey's multiple comparison test. Differences were considered statistically significant at $p < 0.05$ (Figure 7). The antibacterial mechanism of ZnO-functionalized lyocell fabrics (L1 and L2) involves a synergistic multi-pathway action including reactive oxygen species (ROS) generation, Zn^{2+} ion release, and

direct nanoparticle–cell interactions. Unlike pristine lyocell, ZnO deposition introduces active antimicrobial sites. Under ambient moisture, ZnO generates ROS (•OH, O_2•$^-$, H_2O_2), causing oxidative damage to bacterial membranes, proteins, and DNA, ultimately leading to cell death. Simultaneously, released Zn^{2+} ions penetrate bacterial cells, disrupt membrane integrity, inhibit enzyme activity, and disturb ionic balance. Direct nanoparticle contact further induces membrane deformation and leakage of intracellular contents.

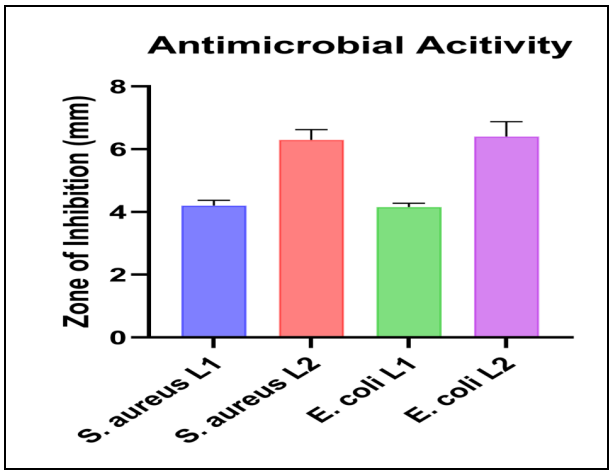

Fig. 7: Antimicrobial activity of ZnO-treated lyocell

The higher antibacterial performance of L2 compared to L1 is attributed to increased ZnO loading, resulting in greater nanoparticle density, enhanced ROS production, and higher Zn^{2+} release. Additionally, the rough, nano-textured surface improves bacterial interaction. Gram-negative *E. coli* shows slightly higher susceptibility due to its thinner cell wall structure. Quantitative antibacterial assessment revealed a clear concentration-dependent performance of ZnO-treated lyocell fabrics against both *Staphylococcus aureus* and *Escherichia coli*. The Pristine lyocell exhibited a bacterial load of 1.2×106 CFU/mL. The 0.25 M sample (L1) reduced the bacterial count to 3.0×105 CFU/mL, corresponding to a 75 % reduction, whereas the 0.5 M sample (L2) further decreased it to 5.0×104 CFU/mL, achieving a 95.8% reduction. Similar trends were observed for *Escherichia coli*, indicating broad-spectrum antibacterial activity. These findings confirm that increased ZnO loading enhances nanoparticle deposition and significantly improves bactericidal efficiency.

3.5 UPF Analysis

The ultraviolet (UV) protection performance of pristine lyocell (L) and ZnO-functionalized fabrics (L1, L2) was evaluated using AATCC 183:2010. Pristine lyocell showed a low protection UPF of 8.29, indicating limited protection due to its inherent optical transparency in the 290–400 nm region and absence of UV-absorbing chromophores. ZnO incorporation significantly improved UPF to 18.2 (L1) and 26.9 (L2), indicating a concentration-dependent enhancement. This improvement arises from combined UV absorption and scattering mechanisms. ZnO, with a wide band gap (~3.3 eV), absorbs UV radiation through electron excitation, while nanoscale particles scatter photons, reducing transmission. Higher ZnO loading in L2 increases nanoparticle density and surface coverage, forming an effective protective layer and lowering UV transmittance. Uniform nanoparticle distribution and strong bonding with cellulose hydroxyl groups enhance functional efficiency and stability. The nano-textured morphology further improves photon interaction. Although durability was not experimentally tested, in-situ synthesis is known to provide strong nanoparticle anchoring, maintaining antibacterial and UV-protective performance through sustained ROS generation, Zn^{2+} release, and inherent UV absorption–scattering properties.

3.6 Air Permeability

The air permeability of lyocell fabrics decreased after ZnO nanoparticle treatment, from 232 mm/s (L) to 200 mm/s (L1) and 176 mm/s (L2). This reduction is attributed to nanoparticle deposition, which partially blocks inter-yarn pores and creates a denser structure, as confirmed by FESEM analysis. Despite this decrease, the fabrics remain sufficiently breathable. Pristine lyocell provides higher ventilation and moisture dissipation, while ZnO-treated samples maintain acceptable comfort levels. The moderate reduction reflects a balance between breathability and added functionality. Importantly, lower air permeability in L2 enhances UV protection and antimicrobial performance by limiting radiation penetration and microbial entry. Thus, ZnO functionalization introduces controlled structural modification, preserving comfort while improving protective properties. Overall, the treated fabrics demonstrate an effective combination of breathability, UV shielding, and antibacterial functionality, making them suitable for advanced wearable and protective textile applications. The reduction in air permeability after ZnO nanoparticle deposition was statistically significant ($p < 0.05$) when compared with the pristine lyocell fabric, confirming that the observed changes were attributable to the surface modification rather than experimental variability.

4. CONCLUSIONS

This study successfully demonstrated a citric acid-assisted in-situ synthesis approach for the functionalization of lyocell fabric with ZnO nanoparticles, providing an environmentally friendly strategy for developing multifunctional textiles without the use of conventional polymeric binders. The findings contribute to the growing body of knowledge on sustainable surface engineering of regenerated cellulose fibres by establishing a clear relationship between ZnO

precursor concentration, nanoparticle formation, and the resulting multifunctional performance.

The developed ZnO-functionalized lyocell fabric exhibited a balanced combination of enhanced antibacterial activity, improved ultraviolet protection, and acceptable air permeability, highlighting the potential of in-situ nanostructure formation for producing high-value functional textiles. The use of citric acid as a sustainable crosslinking agent further supports the development of greener textile finishing technologies with reduced environmental impact.

From an industrial perspective, the proposed finishing process is simple, scalable, and compatible with conventional textile wet-processing operations, making it suitable for applications in medical textiles, protective clothing, sportswear, outdoor apparel, and other technical textile products where antimicrobial performance and UV protection are essential.

Overall, this work demonstrates that sustainable in-situ ZnO nanoparticle functionalization offers an effective pathway for producing next-generation multifunctional lyocell textiles, supporting the transition toward environmentally responsible, high-performance technical textile materials.

FUNDING

This research received no specific grant from any funding agency in the public, commercial, or not-for-profit sectors.

CONFLICTS OF INTEREST

The authors declare that there is no conflict of interest.

COPYRIGHT

This article is an open-access article distributed under the terms and conditions of the Creative Commons Attribution (CC BY) license (http://creativecommons.org/licenses/by/4.0/).

REFERENCES

Abou, E. T. M., Elsisi, H., Elsayad, G., Elhadad, H. and Plutino, M. R., Recent Advances in Functionalization of Cotton Fabrics with Nanotechnology, *Polym.*, 14(20), 4273 (2022). https://doi.org/10.3390/polym14204273

Blessymol, B., Kalaiselvi, V., Yasotha, P. and Gopi, S., Comparative Study of Chemically and Green Synthesized Titanium Dioxide Nanoparticles using Leucas aspera Leaf Extract, *J. Environ. Nanotechnol.*, 12(3), 10-13(2023). https://doi.org/10.13074/jent.2023.09.233471

Cichosz, S. and Masek, A., IR Study on Cellulose with the Varied Moisture Contents: Insight into the Supramolecular Structure, *Mater.*, 13(20), 4573 (2020). https://doi.org/10.3390/ma13204573

Djafari, P. S. R., Shojaeiarani, J. and Chabot, B., Recent advances in isolation, characterization, and potential applications of nanocellulose-based composites: A comprehensive review, *J. Nat. Fibers.,* 20(1), 2146830 (2023). https://doi.org/10.1080/15440478.2022.2146830

Geminiani, L., Campione, F., Corti, C., Luraschi, M., Motella, S., Recchia, S. and Rampazzi, L., Differentiating between Natural and Modified Cellulosic Fibres Using ATR-FTIR Spectroscopy, *Heritage*, 5(4), 4114-4139 (2022) https://doi.org/10.3390/heritage5040213

Ivanova, O., Röder, T., Innerlohinger, J. A., Rosenau, T. and Hettegger, H., The chemistry of the lyocell process: a critical review of recent developments, *Cellulose*, 33(8), 4435–4459 (2026). https://doi.org/10.1007/s10570-026-07081-5

Jalali, E., Erasmus, E., Schutte-Smith, M. and Visser, Hendrik, G., Fixation of nanoparticles on fabric: Applications in general health management, *Mater. Today. Commun.*, 41, 110577 (2024). https://doi.org/10.1016/j.mtcomm.2024.110577

Javed, A., Wiener, J., Tamulevičienė, A., Tamulevičius, T., Lazauskas, A., Saskova, J. and Račkauskas, S., One Step In-Situ Synthesis of Zinc Oxide Nanoparticles for Multifunctional Cotton Fabrics, *Mater.*, 14(14), 3956 (2021). https://doi.org/10.3390/ma14143956

Liu, Y. and Kim, H.J., Fourier Transform Infrared Spectroscopy (FT-IR) and Simple Algorithm Analysis for Rapid and Non-Destructive Assessment of Developmental Cotton Fibers, *Sensors*, 17(7),1469 (2017). https://doi.org/10.3390/s17071469

Mondal, S., Nanomaterials for UV protective textiles, *J. Ind. Text.,* 51(4), 5592S-5621S (2022). https://doi.org/10.1177/1528083721988949

Mpofu, N. S., Mwasiagi, J. I., Mecha, C. A. and Nganyi, E. O., Characterization and Performance Evaluation of Cotton Fabrics Functionalized via In Situ Green Synthesis of Silver Nanoparticles Using Solanum tuberosum Peel Extract, *Polym.,* 17(19), 2598 (2025). https://doi.org/10.3390/polym17192598

Periyasamy, A. P., Natural dyeing of cellulose fibers using syzygium cumini fruit extracts and a bio-mordant: A step toward sustainable dyeing, *Sustain. Mater. Technol.,* 33, e00472 (2022). https://doi.org/10.1016/j.susmat.2022.e00472

Ravi, P. and Babu, S., Recent development in plant-mediated zinc oxide nanoparticles with biomedical applications, *Chem. Phys. Impact.*, 10, 100870 (2025). https://doi.org/10.1016/j.chphi.2025.100870

Rodrigues, L., Medeiros, J., Marques, R. and Silva, C. J., Lyocell-Based Nonwovens: Mechanical Performance and Biodegradation Analysis, *Tex.*, 5(2), 20 (2025). https://doi.org/10.3390/textiles5020020

Sadannavar, M. K., Periyasamy, A., Islam, S. R., Shafiq, F., Dong, X. and Zhao, T., Natural Dyeing and Antimicrobial Functionalization of Wool Fabrics Dyed with Chinese Dragon Fruit Extract to Enhance Sustainable Textiles, *Sustainability*, 16(16), 6832, (2024). https://doi.org/10.3390/su16166832

Shilo, N. S. H. and Tarangini, K., A review on augmentation of natural fabric materials with novel bio/nanomaterials and their multifunctional perspectives, *Hybrid. Adv.,* 2, 100020 (2023). https://doi.org/10.1016/j.hybadv.2023.100020

Sowri, B. K., Ramachandra, R. A., Sujatha, C., Venugopal, R. K. and Mallika, A. N., Synthesis and optical characterization of porous ZnO, *J. Adv. Ceram.,* 2(3), 260-265 (2013). https://doi.org/10.1007/s40145-013-0069-6

Verbič, A., Gorjanc, M. and Simončič, B., Zinc Oxide for Functional Textile Coatings: Recent Advances, *Coatings*, 9(9), 550 (2019). https://doi.org/10.3390/coatings9090550

Verbič, A., Šala, M., Jerman, I. and Gorjanc, M., Novel Green In Situ Synthesis of ZnO Nanoparticles on Cotton Using Pomegranate Peel Extract, *Mater.*, 14(16), 4472 (2021). https://doi.org/10.3390/ma14164472

Wang, X., Wang, S., Li, Y., Jin, X. and Dong, C., Preparation and properties of low fibrillated antibacterial Lyocell fiber, *Arab. J. Chem.,* 17(4), 105658 (2024). https://doi.org/10.1016/j.arabjc.2024.105658

Wendler, F., Schulze, T., Bauer, J. and Redlingshöfer, B., Bioactive Lyocell Fibers with Inherent Antibacterial, Antiviral and Antifungal Properties, *Mol.*, 29(9), 2054 (2024). https://doi.org/10.3390/molecules29092054

Xu, H., Yan, S., Gerhard, E., Xie, D., Liu, X., Zhang, B., Shi, D., Ameer, G. A. and Yang, J., Citric Acid: A Nexus Between Cellular Mechanisms and Biomaterial Innovations, *Adv. Mater.,* 36(32), 2402871 (2024). https://doi.org/10.1002/adma.202402871